JMEPEG (2012) 21:1763–1771
DOI: 10.1007/s11665-011-0073-3

1059-9495/$19.00

On the Critical Technological Issues of Friction Stir Welding T-Joints of Dissimilar Aluminum Alloys

A. Astarita, A. Squillace, A. Scala, and A. Prisco

(Submitted June 6, 2011; in revised form September 1, 2011)

In this article, friction stir welded T-joints of innovative dissimilar aluminum alloys have been produced and tested with the aim to investigate the feasibility of using this joining technique, in this configuration, in the aerospace field with the final aim to save weight. The introduction of both this new welding technique and innovative alloys, such as AA 2198 and AA 6056, could allow making lighter and stronger structures. Some experiments, carried out previously, have shown that the fixturing device, the tool geometry, and the tilt angle play a significant role in the joint soundness. A wide experimental characterization has been carried out on FSW T-joints of AA 6056 T4 extrudes to AA 2198 T3 rolled plates. The results attained allow to put in evidence some critical issues on the investigated configuration and can be considered as a further acquired knowledge in the understanding and the design of friction stir processes.

Keywords AA 2198, friction stir welding, mechanical properties, stress corrosion cracking

1. Introduction

Nowadays the fiber reinforced materials are finding more and more widespread use in aeronautic field due to their features of lightness, high strength, and flexibility of manufacturing systems. The only way for metals to remain competitive for the aerospace applications is to improve new technologies and alloys to realize lighter and more resistant structures. The development of new alloys (lighter and stronger) and technologies will allow using metals also in the future for aerospace applications. In this scenario, the research activity has a fundamental importance, and the key point is to work simultaneously on both innovative materials and new technologies that allow to obtain the best performances with the innovative alloys.

The fuselage of an airplane consists of three fundamental parts: skin, stringer, and frame; these parts are actually joined by means of rivets. The riveting processes involve a great amount of drawbacks for the aero structures, all resulting in a weight increment. Notwithstanding the use of riveting is unavoidable due to the inadequate weldability of the high resistance heat treatable aluminum alloys (2xxx and 7xxx series) used in the aeronautic by means of the conventional fusion welding techniques. The introduction of the friction stir welding (FSW) at the beginning of the nineties allowed a considerable improvement in the welding of these alloys due to the solid state welding, i.e., no melting occurs, as seen in the review of Mishra et al. (Ref 1). T-joints can be made, using FSW, with two different configurations: the former described by Dubourg et al. (Ref 2) and the latter described by Fratini et al. (Ref 3). In the FSW of T-joints, as reported in both the papers of Fratini et al. (Ref 3, 4), a specially designed rotating tool is plunged, with a given tilt angle, into the clamped blanks and then it is moved along the welding line. In the FSW, the heat source is mainly obtained by the frictional force work and, to some extent, by the deformation work during tool movement resulting into heat along the welding line. In this way, depending on tool geometry and dimensions, the tool rotation speed (R) and welding speed (Vf) are the main process variables determining the specific thermal input conferred to the joint. The generated heat flux induces local material softening but no melting is achieved, preventing undesired metallurgical defects such as inclusions, pores, etc. that can dramatically affect the joint performance. Again, the tool movement activates the material plastic flow, as studied (Ref 5, 6). Consequently, FSW main process parameters govern the metallurgy of the weld bead (Ref 7, 8). With reference to a butt joint, in the core of the bead, the so called nugget zone is observed where the original grain and subgrain boundaries appear to be replaced with fine, equiaxed recrystallized grains characterized by a nominal dimension of a few micrometers. All around the nugget first a thermo-mechanical affected zone (TMAZ) is created, where the material experiences the effects of both the stirring mechanical action of the tool pin and the heat generated by friction. Then a conventional heat affected zone (HAZ) is generated due to high temperatures that in turn is surrounded by the parent unaffected material.

It should be outlined, as reported by Fratini et al. (Ref 9) that the existing knowledge on FSW process of butt joints is not immediately extendable to the T-joints. First of all in the butt joints the surface to be welded is vertical, while in T-joints it is horizontal and placed at the bottom of the top blank to be welded, i.e., the skin in our case study. This means that in the former case the weld bead is created by stirring the two materials staying, respectively, at the left and at the right of the tool axis: this stirring action is easily performed thanks to the

A. Astarita, A. Squillace, and **A. Scala**, Department of Materials and Production Engineering, University of Naples Federico II, Naples, Italy; and **A. Prisco**, Operations—Manufacturing Research & Development, ALENIA Aeronautica S.p.A, Turin, Italy. Contact e-mail: antonello.astarita@unina.it.

rotation of the tool itself. On the contrary, in the latter case, the weld bead is created by stirring the two materials staying, respectively, upside and downside: this stirring action cannot be simply achieved by the tool rotation, as in the previous case, but it is realized by means of the synergy of different tool characteristics such as a truncated cone shape of the pin and a threaded pin and the setting of an appropriate tilt angle, usually greater than those commonly adopted in the butt joints, as reported by Fratini et al. (Ref 4). In the T-joint configuration, a dedicated fixture device is needed to constrain the stringer; such device has two fillet radii, one for each side of the joints, corresponding to the desired radii to be created between skin and stringer in the final welded manufacture. These radii have to be filled by the softened material. Therefore, a forging action is needed to force the skin and the stringer material in fulfilling the radii so resulting in the radii of the T-joint. Such need means that, given the materials to be welded, the process parameters that have been demonstrated to be effective in the butt joint configuration could not be appropriate for the T-joint configuration. In particular, the tool geometry, the welding, and the rotating speed have to be re-determined for T-joints to achieve an efficient material flow and, finally, the bonding in the FSW process.

Beyond new technologies, new alloys have being developed, lighter and stronger than conventional ones, such as the new aluminum-lithium alloys. The lithium, for metallurgical reasons, is used together other usual alloying elements, an example is the AA 2198, containing Copper as main alloying element. Al-Li alloys have higher Young modulus and lower density than the traditional ones. By applying new technologies on innovative alloys it is possible to achieve both lighter and stronger structures that can be competitive with new composite structures.

The aim of the present work is to study the FSW of an AA 6056 stringer on an AA 2198 T3 skin. The welding configuration being the T-joint. The authors intend to provide an overview of main characteristics of this kind of joint: the macro- and micro-structural ones, the mechanical properties in different loading conditions and, to conclude, how these characteristics govern the behavior of the joint itself in an aggressive environment, as pointed out by Padovani et al. (Ref 10).

2. Materials and Methods

2.1 Joints Realization

In this work an innovative Al-Cu-Li alloy, the AA 2198 T3 in rolled sheet form, has been used coupled to an AA 6056 T4 in extruded form. Tables 1 and 2 report the chemical compositions of the two alloys.

These two alloys have been realized specifically for the aeronautic industry with the aim to provide new alloys having mechanical properties similar, or even superior, to the conventional ones, but with an enhanced weldability.

Due to the presence of lithium, the AA 2198 T3 shows a higher *E* modulus and a lower density than the traditional Al-Cu alloys. Table 3 reports main mechanical properties of the alloy in the T3 condition in both LL and TL directions: it is possible to appreciate a significant difference of values attained along the two directions due to a remarkable anisotropy of aluminum alloys rolled sheet containing lithium, as seen in Ref 11.

Table 1 Chemical composition of AA 2198

	Si	Fe	Cu	Mn	Mg	Cr	Zn	Zr	Li	Ag
Min			2.90		0.25			0.04	0.80	0.10
Max	0.08	0.10	3.50	0.50	0.80	0.05	0.35	0.18	1.10	0.50

Table 2 Chemical composition of AA 6056

	Si	Fe	Cu	Mn	Mg	Cr	Zr + Ti	Zn
Min	0.70		0.5	0.4	0.6			0.1
Max	1.3	0.50	1.1	1.0	1.2	0.25	0.2	0.7

Table 3 Main mechanical properties of AA 2198 T3 in L and LT directions

AA 2198 T3	Yield strength, MPa	Tensile strength, MPa	Elongation, %
L	315	375	15
LT	275	370	15

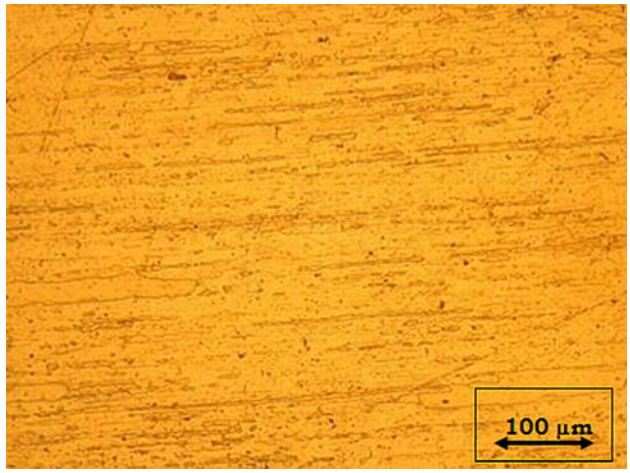

Fig. 1 Microstructure of AA 2198 T3

In Fig. 1, it is possible to see the microstructure of the alloy used in this experimentation: the presence of lithium results in a very elongated grain structure, responsible for the above-mentioned anisotropy.

The joints have been made starting from AA 2198 T3 rolled sheets having the following dimensions: thickness 3 mm, length 500 mm, and width 230 mm. Rectangular extruded of AA 6056 T6 (having a thickness of 6 mm, a length of 500 mm, and a width of 30 mm) have been joined by friction stir welding on above sheets. The weld has been made along the rolling direction of the skin. In Fig. 2, it is reported the welding configuration used for these joints.

A steel tool has been used having the geometry reported in Fig. 3, with main features reported in Table 4.

A dedicated fixture has been designed to constrain both the skin and the stringer during the welding.

The main process parameters adopted are: a rotational speed of 830 rpm, a welding speed of 40 mm/min, and a tilt angle of

2°. These parameters have been chosen according to preliminary tests carried out to find welding process parameters resulting in sound welds.

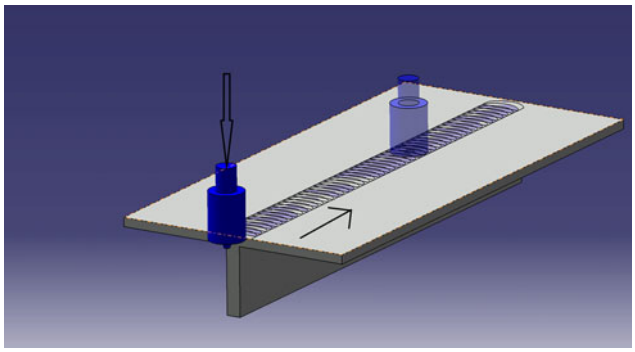

Fig. 2 Welding configuration: the two arrows indicate plunging direction and welding direction

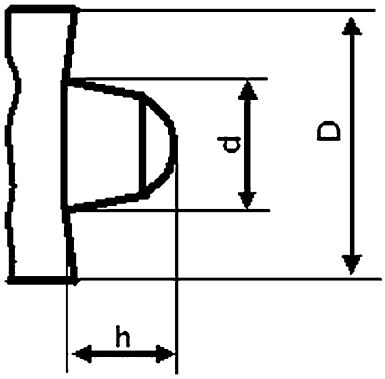

Fig. 3 Geometry of the tool

Table 4 Tool main dimensions

D, mm	*d*, mm	*h*, mm
17.5	4.5	4

2.2 Metallographic Investigations

The specimens for metallographic observations have been prepared according to the international standards: ASTM E3, ASTM E 340, ASTM E 1558 (Ref 12–14).

Both macro- and micrography have been carried out: the former to appreciate the global geometry of the weld bead and the shape and the extension of each characteristic zone of the weld (i.e., the nugget zone, the thermomechanically affected zone, and the heat affected zone) and the possible occurrence of defects; the latter to study the microstructures created by the joining process.

2.3 Mechanical Characterization

In order to investigate the mechanical performances of the joints some mechanical tests were carried out. In particular, two different kinds of tests were carried out: the hoop stress tests and T-pull tests. The two typologies differ in the loading configuration, because each of them has the aim to test a particular feature of the entire joined component. In the hoop stress test the main loaded part is the skin, in fact this test simulates the stresses resulting in the skin as a consequence of the pressurization and depressurization of the fuselage during the working life of the airplane. This test allows mainly to quantify the residual efficiency of the skin, after the thermo-mechanical action experienced during the welding. Figure 4 reports a draw of the specimen used for this test.

The test has been carried out according to the ASTM E8 standard.

The second kind of mechanical test is the T-pull one. In this test, it is simulated a load trying to pull out the stringer from the skin. This test has been carried out according to the standard ASTM E8, and using a universal testing machine but using a particular tooling to grab the specimen and transmit the load. The sample used have the same geometry of the samples used for the hoop stress test, but is different the direction of load application, as is reported in Fig. 5.

In this test the skin is clamped in the device, the stringer is grabbed by the testing machine.

On the each tested specimens a study on the fracture surfaces has been conducted, to estimate the failure modality and the causes of the failures.

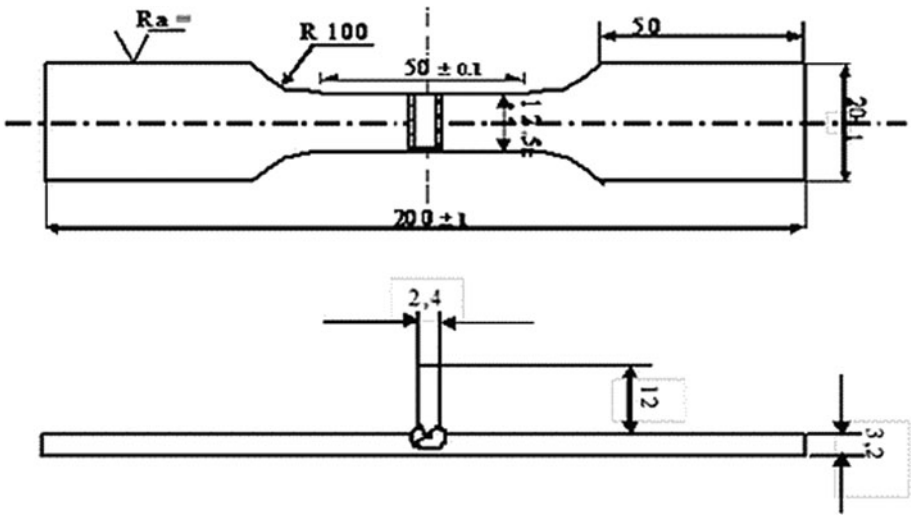

Fig. 4 Hoop stress specimen (the dimension in millimeters)

2.4 SCC Test

In order to better predict the behavior of the joints in service, Stress Corrosion Cracking (SCC) tests have been carried out too. This test allows to evaluate the synergic effects of a mechanical load and of an aggressive environment, so simulating realistic severe service conditions. This test has been conducted according to the international standards: ASTM G44, ASTM G47, ASTM G49 (Ref 15–17).

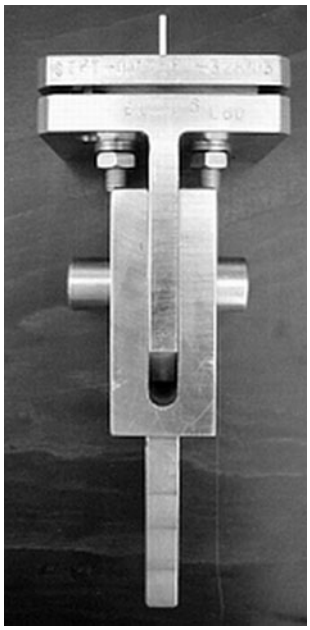

Fig. 5 T-pull load loading device

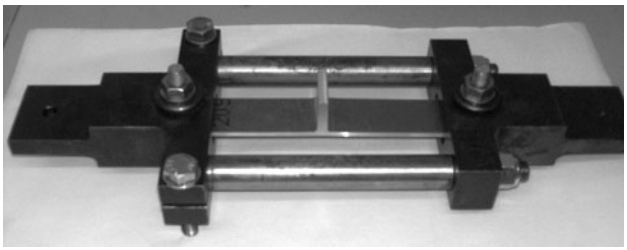

Fig. 6 SCC fixturing device

Table 5 Sample designation in SCC test

Sample description	Designation
Pre-strained, advancing upside	PA
Pre-strained, retreating upside	PR
Unstrained, advancing upside	UA
Unstrained, retreating upside	UR

For this test the specimen geometry is the same used for the traction one, the only difference is the width that in this case is 30 mm.

The specimen is pre-strained up to a strain value corresponding to 80% of ultimate tensile strength (such a value is measured during static tensile test). This has been made by means of a dedicated device showed in Fig. 6.

Eight specimens, mounted in the above device, have been put in the test machine that is a particular machine that periodically dips the specimens in the aggressive environment (in this case a 3.5% in weight of NaCl water solution) for 10 min every hour; the whole test has a duration of 30 days.

The above device imposing the strain to the specimen is made of steel so to avoid corrosion problem or any electrochemical interference between the specimen and the device itself the two ends of each specimen have been coated with enamel and the entire surface of the steel device coated with wax. The correct electrical insulation of the specimen with respect to the steel device has been verified by means of electrical universal tester.

In order to avoid the consumption of oxygen in the bath during the tests, air is continuously insufflated in the bath itself during the period of 50 min per hour in which the specimens are out of the bath.

Taking into account the dissymmetry of the specimens (in a friction stir weld it is possible to discern two different zone named the advancing side and the retreating side, as reported in Ref 1) with different microstructures, this test has been carried out in two different configurations: in the former the specimens have been put in the bath with the advancing side upside, in the latter the specimens have been immersed in the opposite verse. This because when the specimens are raised up from the bath, a certain amount of aggressive solution remains trapped on the upper side of the specimen (the stringer acts as a spoon). Further unstrained specimens have been tested too in order to accurately check the influence of the mechanical stress, as suggested by international standards ASTM G47 (Ref 16). Since the testing machine allows to test simultaneously 8 specimens, during each test four different samples have been tested (each sample consisting of 2 specimens), according to Table 5.

The test results have been evaluated by means of visual inspection and micro- and macro-observations by means of light microscopy. Then the specimens have been sectioned, mounted, polished, etched, and observed following the methodology reported in section 2.2 (Table 6, 7).

Table 6 Results of hoop stress test

Specimen	Thickness, mm	Width, mm	Resistant area, mm^2	Yield strength, MPa	Ultimate tensile strength, MPa	Elongation, %	Young modulus, GPa
1	3.190	12.45	39.90	211	296	2.93	70.34
2	3.200	12.47	39.90	214	268	2.20	71.69
3	3.170	12.35	39.15	211	235	1.59	73.71
4	3.190	12.54	40.00	209	288	2.65	72.76
5	3.160	12.48	39.44	221	271	2.41	73.41

Table 7 Mean values and standard deviation of main mechanical characteristics

	Yield strength, MPa	Ultimate tensile strength, MPa	Elongation, %	Young modulus, GPa
Mean value	213.3	271.8	2.4	72.4
Standard deviation	4.6	23.4	0.5	1.4

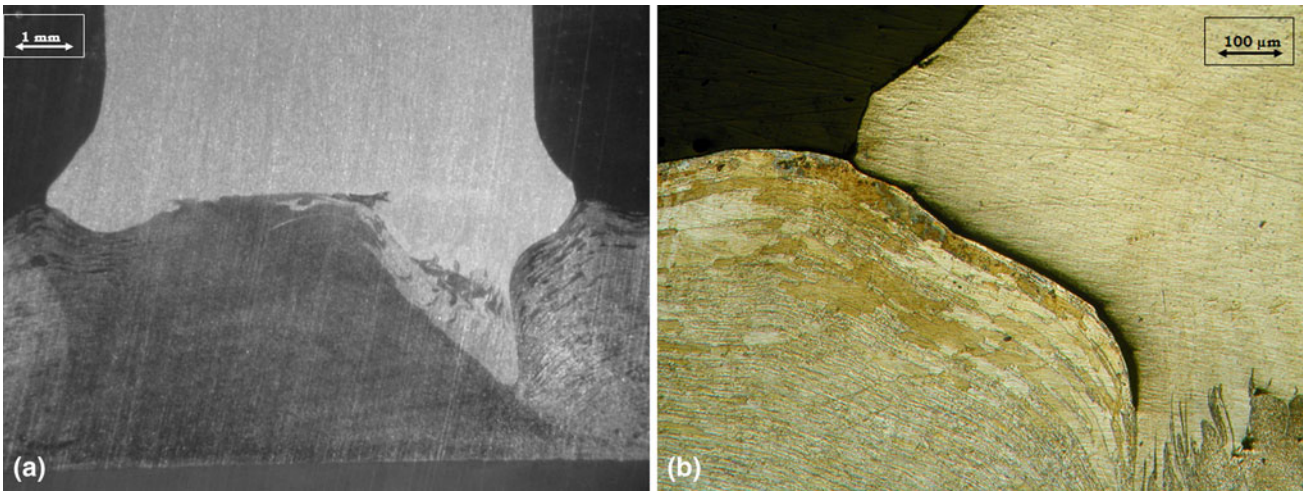

Fig. 7 Macrograph of the T joint (a) and kissing bond between stringer and skin (b)

Fig. 8 Particular of the tunnel in the nugget, 15×

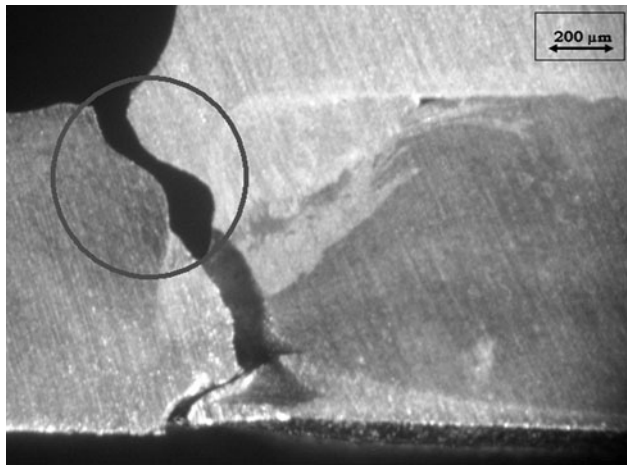

Fig. 9 Fracture line in hoop stress test

3. Results and Discussion

3.1 Metallographic Investigations

First it is possible to show the macrographs of the joint to evaluate the aspect of the welds, the presence of macro-defects and the stirring experienced by the material. Figure 7(a) shows the joint after polishing and electrochemical etching (Keller's reagent for 20 s).

It can be noted that the nugget in the T-joint configuration appears unacceptable: it has been noticed a poor mixing of the skin material with the stringer one. Kissing bond defects are evident in the connection zone of the stringer to the skin, see Fig. 7(b). This kind of defect could result in catastrophic failure under both mechanical and electrochemical solicitations; since it could act as a preferential site for crack initiation and propagation. Furthermore, there is a large tunnel in the core of the bead and passing through the entire joint. This type of defect has been detected in all the analyzed specimens.

The joints have been also observed at the microscopic level to acquire additional information on the microstructure of the joint. Figure 8 shows a particular of the defect in the skin-stringer connection zone. Furthermore, in the same figure, it can be appreciated the lack of metallurgical continuity between skin and stringer and a general grain size refinement of the skin.

3.2 Mechanical Characterization

It is possible to calculate the mean values and the standard deviation for yield strength and ultimate tensile strength.

Referring to the mechanical properties of the base material (AA 2198 T3) it is possible to calculate the efficiency of the joint, defined as the ratio of the tensile strength of the joint to the tensile strength of the base material. This parameter is very important since allows to quantify the influence of the welding process on the mechanical properties of the base material. According to the mechanical properties of the base material reported in Table 2, it is possible to calculate the efficiency of the joint, as reported in Table 8.

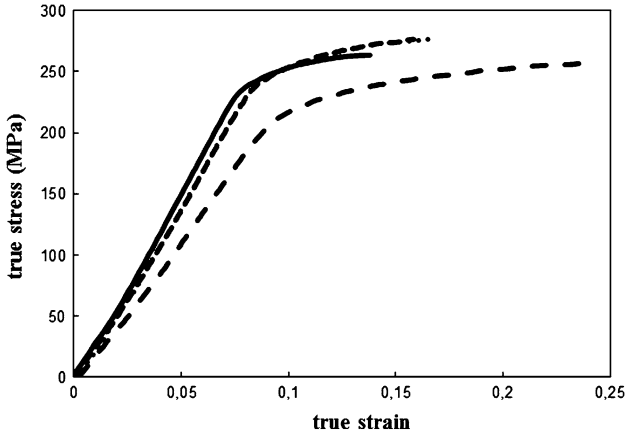

Fig. 10 True stress vs. true strain curves of the hoop stress test

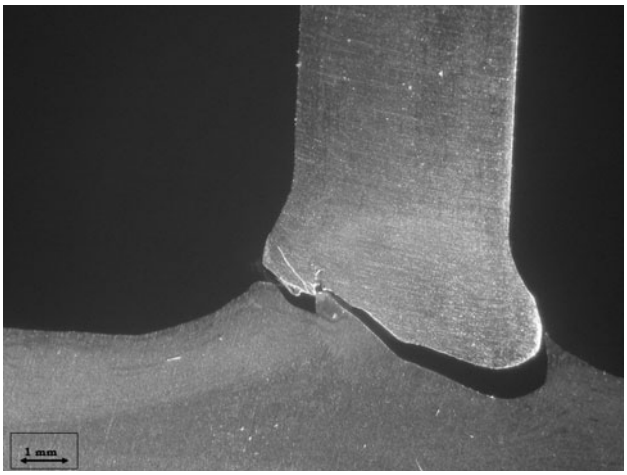

Fig. 11 Fractography of T-pull specimen

The efficiency appears quite low if compared to the efficiency achievable, for the T-joint configuration under investigation, with Laser Beam Welding, as seen in Ref 18. In making joints with this geometry by means of friction stir welding the entire thickness of the skin experiences the tool action: the tool fully plunges in the skin, and partially in the stringer, during the welding process, moves along the welding line and, since the alloy is an heat treatable one, this causes a loss of the mechanical properties of the skin itself. Conversely in the laser beam welding only a small portion of the thickness is involved in the process and, as a consequence, the remaining portion preserve completely this mechanical properties.

By viewing Fig. 15, it is possible to see both the site in which fracture occurs, the fillet radius between skin and stringer, and fracture line itself. Please note that the fracture occurs in all the specimens in the same way. The kissing bond defect described in the previous paragraph plays a significant role in the fracture occurrence: the circle in Fig. 9, in fact, allows to appreciate how fracture path follows perfectly the kissing bond defect, i.e., the lack of metallurgical continuity induced by such a defect results in a dramatic reduction of the cross section.

Last it is possible to present the true stress-true strain curves to discuss the qualitative behavior of the joints.

It is possible to note an initial elastic behavior, followed by a plastic one up to the final failure of the specimens. Necking phenomenon did not occur in this case.

In Table 9, the results of the T-pull test are reported.

It is possible to see the low values of strength provided by the joints in this new loading condition.

Furthermore, in this case, it is not possible to do any comparison with parent material and, as a consequence, no joint efficiency can be calculated. The only comparison that could be made is that with the conventional riveted T-joints.

Some macrographs of the fracture path have been taken to better understand the failure mechanism (Fig. 10).

From Fig. 11, it is evident how the failure path follows the main welding defects observed and described in the previous paragraphs, i.e., the kissing bond and the tunnel. Thanks to this

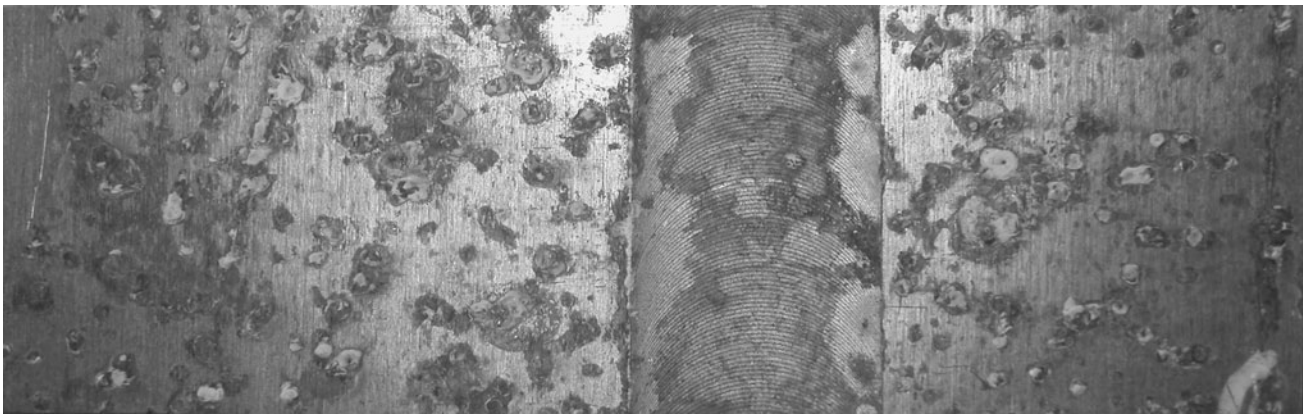

Fig. 12 Pre-strained specimen after the SCC test

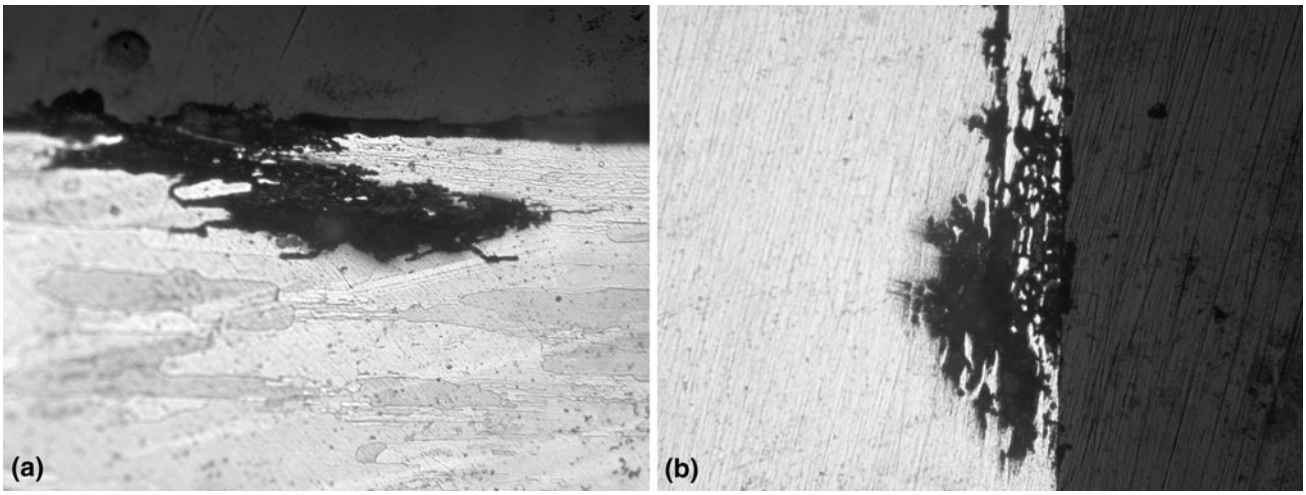

Fig. 13 (a) 300× pit on skin base material and (b) 500× pit on stringer base material

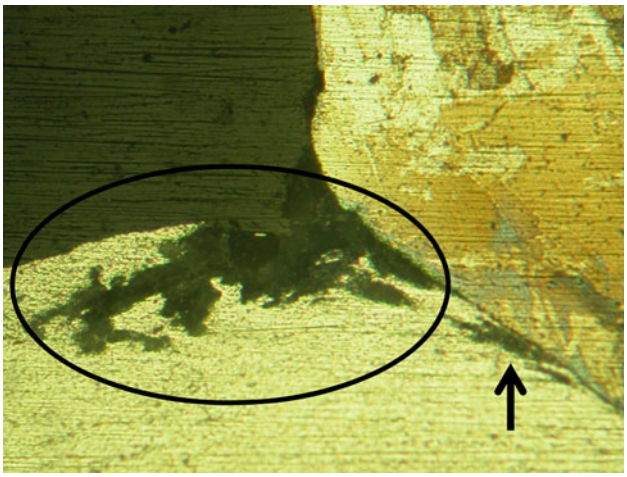

Fig. 14 Corrosion close to kissing bond defect, the stringer is the brighter part on the bottom side

Table 8 Joints efficiency in hoop stress tests

Specimen	UTS, MPa	Efficiency, %
1	296	69
2	268	62
3	235	55
4	271	63
5	288	67
Mean values	271	63

kind of test (i.e., the T-pull one), the inadequate stirring of material realized in the configuration under investigation, resulting in a lack of metallurgical continuity within the weld bead, governs totally the behavior and the performance of the joint.

3.3 SCC Test

After 30 days of testing no failures have been observed in the tested specimens; anyway this does not allow to affirm that the joints are not susceptible at SCC phenomena. Then

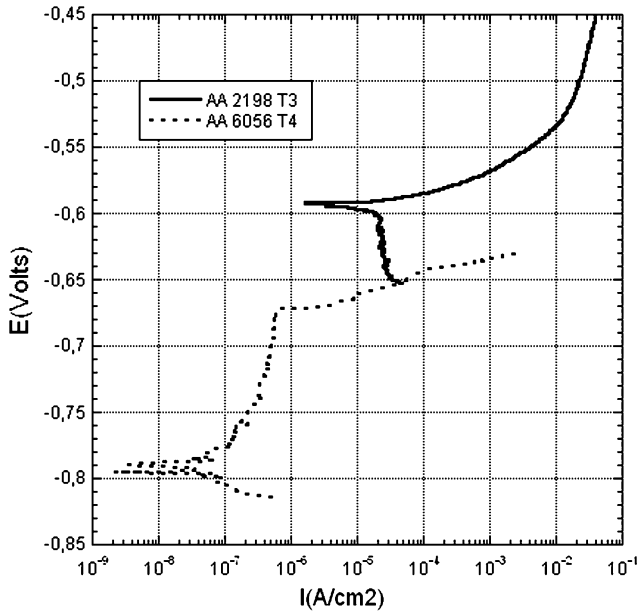

Fig. 15 Polarization curve for AA 2198 T3 and 6056 T4

metallographic observations have been conducted to better understand and try to interpret the results of the test.

Figure 12 shows a specimen after the test: it is possible to see numerous pits, as expected, on the surface. In the same figure, the absence of pits on the top surface of the weld bead allows to appreciate the better corrosion resistance of the weld bead itself with respect to the adjacent base material. By means of microscopic observations of the cross section of the same specimen, see Fig. 13, it is possible to see that these pits are of "under cutting" kind, as studied by Roberge (Ref 19).

From Fig. 13, it is possible to appreciate how large pits are how they tend toward exfoliation. A possible interpretation of the tendency to exfoliation of pre-strained specimens could be found in the strong anisotropy, as described above, of both the skin rolled sheet and the extruded stringer.

Obviously, the main differences in pits shape and dimensions in skin and stringer are due to both the different grain

Table 9 Results of the T-pull test

Specimen	Thickness, mm	Width, mm	Area, mm^2	Max load, kN	Strength, MPa
1	3.14	30.0	94.20	11.965	127
2	3.14	30.1	94.51	17.824	189
3	3.14	30.0	94.20	14.970	159
4	3.14	29.8	93.57	17.694	189
5	3.14	29.3	91.97	14.220	155
Mean value					164
Standard deviation					26

structures, being the skin a rolled sheet and the stringer an extruded part, and the different chemical compositions. What's more, as usual in this kind of alloys, it is possible to see a further form of corrosion following the grain boundaries: intergranular corrosion. This last form of corrosion, as expressly described by the international standard ASTM G47, can be attributed to the effects of stress corrosion cracking.

In Fig. 14 it is possible to see how the kissing bond defects between skin and stringer, described in the previous paragraphs, acts as a preferential site for localized corrosion phenomena occurrence.

Such action results in two different corrosion forms: crevice and galvanic corrosion. The former indicated by the arrow in Fig. 14 and the latter indicated by a circle in the same figure. Both forms are promoted by the presence of aqueous solution remaining on the stringer top surface during the emersion period within a single cycle of SCC test and attack exclusively the stringer, made by AA 6056. On the contrary the AA 2198, in this zone, appears intact. This is due to a phenomenon of galvanic coupling between the two alloys promoting corrosion on the alloy characterized by lower corrosion potential. To this scope standard polarization curve, in according with ASTM G5 (Ref 20), tests have been carried out on the two alloys under investigation. Results are reported in Fig. 15: the AA 6056 has an open circuit potential lower than the AA 2198 T3, then in a galvanic coupling the former alloy corrodes. For the same reasons the crevice corrosion form seen in Fig. 14 attack the AA 6056.

Similar forms of corrosion have been observed in the unstrained specimens too, even if in this case they appear less severe.

4. Conclusions

On the basis of the experimental characterization carried out on aluminum alloys friction stir welded T-joints, the following conclusions can be drawn:

- In the configuration under investigation, the material stirring, as described in the introduction, appears inadequate and results in some critical defects, kissing bonds over all. Such defects occur mainly in the core of the nugget zone and in the radii between skin and stringer. Kissing bonds in the radii play a critical role in both mechanical and electrochemical behaviors, fully governing performances attained by the joints.
- The complex geometry to realize, the high forces opposed by the material to the deformation and, as a consequence, the need to rigidly constrain pieces to be joined results in a heavy and strictly dedicated fixturing device. Furthermore, this means an increment of costs and manufacturing time.
- Static mechanical properties, in both hoop stress and T-pull loading conditions, are not fully satisfying due to the intrinsic limits related to the combination of the welding process and configuration, as described previously; the above-mentioned kissing bonds defects occurrence contributes to get worse the performances of the joints.
- SCC tests allow to put in evidence, one more time, the critical issues related to the welding of dissimilar heat treatable aluminum alloys. Kissing bonds defects emphasize such a problem, promoting crevice corrosion, in addition to the expected galvanic one.

Acknowledgment

Authors acknowledge Alenia Aeronautica S.p.A for providing materials to make joints and supporting research activity.

References

1. R.S. Mishra and Z.Y. Ma, Friction Stir Welding and Processing, *Mater. Sci. Eng. R*, 2005, **50**, p 1–78
2. L. Dubourg, A. Merati, and M. Jahazi, Process Optimisation and Mechanical Properties of Friction Stir Lap Welds of 7075-T6 Stringers on 2024-T3 Skin, *Mater. Des.*, 2010, **31**, p 3324–3330
3. L. Fratini, G. Buffa, L. Filice, and F. Gagliardi, FSW of AA6082–T6 T-Joints: Process Engineering and Performance Measurement, *J. Eng. Manuf. Pt B*, 2006, **220**(5), p 669–676
4. L. Fratini, F. Micari, A. Squillace, and G. Giorleo, Experimental Characterization of FSW T-Joints of Light Alloys, *Key Eng. Mater.*, 2007, **344**, p 751–758
5. M. Guerra, C. Schmidt, L.C. McClure, L.E. Murr, and A.C. Nunes, Flow Patterns During Friction Stir Welding, *Mater. Charact.*, 2003, **49**, p 95–101
6. C.G. Rhodes, M.W. Mahoney, W.H. Bingel, R.A. Spurling, and C.C. Bampton, Effects of Friction Stir Welding on Microstructure of 7075 Aluminum, *Scripta Mater.*, 1997, **36**(1), p 69–75
7. J.Q. Su, T.W. Nelson, R. Mishra, and M. Mahoney, Microstructural Investigation of Friction Stir Welded 7050-T654 Aluminium, *Acta Mater.*, 2003, **51**, p 713–729
8. M. Peel, A. Steuwer, M. Preuss, and J.P. Withers, Microstructure, Mechanical Properties and Residual Stresses as a Function of Welding Speed in Aluminium AA5083 Friction Stir Welds, *Acta Mater.*, 2003, **51**(16), p 4791–4801
9. L. Fratini, G. Buffa, and R. Shivpuri, Influence of Material Characteristics on Plastomechanics of the FSW Process for T-Joints, *Mater. Des.*, 2009, **30**(7), p 2435–2445

10. C. Padovani, L. Fratini, A. Squillace, and F. Bellucci, Electrochemical Analysis on Friction Stir Welded and Laser Welded 6XXX Aluminium Alloys T-Joints, *Corros Rev*, 2007, **25**(3–4), p 475–489
11. R.S. James, *Aluminium-Lithium Alloys, Metals Handbook*, Vol 2, 10th ed., ASM International, Materials Park, OH, 1990, p 178–199
12. ASTM E3 Standard Guide for Preparation of Metallographic Specimens
13. ASTM E 340 Test Method for Macroetching Metals and Alloys
14. ASTM E 1558 Guide to Electrolytic Polishing of Metallographic Specimens
15. ASTM G 44 Standard Practice for exposure of Metals and Alloys by Alternate Immersion in Neutral 3.5% Sodium Chloride Solution
16. ASTM G 47 Standard Test Method for Determining Susceptibility to Stress Corrosion Cracking of 2xxx and 7xxx Aluminium Alloys Products
17. ASTM G 49 Standard Practice for Preparation and Use of Direct Tension Stress Corrosion Test Specimens
18. A. Prisco, F. Acerra, F. Bellucci, A. Squillace, C. Pirozzi, U. Prisco, and G. Giorleo, LBW of Similar and Dissimilar Skin-Stringer Joints. Part I: Process optimization and Mechanical Characterization. *Adv. Mater. Res*., 2008, **38**, p 306–319. ISSN: 1022-6680: Trans Tech Publications (Switzerland)
19. P.R. Roberge, *Handbook of Corrosion Engineering*, McGraw-Hill, New York, 2000
20. ASTM G5 Standard Reference Test Method for Making Potentiostatic and Potentiodynamic Anodic Polarization Measurements